ATION PAGE

DATE 13 Oct 91

3. REPORT TYPE AND DATES COVERED: Journal Article Dec 89 - Sep 91

An Optical Image Segmentor Using Neural Based Wavelet Filtering Techniques

Christopher P. Veronin, Steven K. Rogers, Matthew Kabrisky, Kevin L. Priddy, Kevin W. Ayer, Byron Welsh

Air Force Institute of Technology, AFIT/ENG
Wright-Patterson AFB OH 45433-6583

Wright Laboratory
Avionics Directorate (WL/AARI)

WL-TR-91-1149

Kevin W. Ayer, Capt, USAF (513/255-9614)
Avionics Directorate (WL/AARI)
Wright Laboratory
Wright-Patterson AFB, Ohio 45433-6543

To be published in the February 1992 issue of Optical Engineering

Approved for Public Release, Distribution Unlimited

This paper presents a neural based optical image segmentation scheme for locating potential targets in cluttered FLIR images. The advantage of such a scheme is speed, i.e., the speed of light. Such a design is critical to achieve real-time segmentation and classification for machine vision applications. The segmentation scheme used was based on texture discrimination and employed biologically based orientation specific filters (wavelet filters) as its main component. These filters are the well understood impulse response functions of mammalian vision systems from input to striate cortex. By using the proper choice of aperture pair separation, dilation, and orientation, targets in FLIR imagery were optically segmented. Wavelet filtering is illustrated for glass template slides, as well as segmentation for static and real-time FLIR imagery displayed on a liquid crystal television.

Gabor Transforms, Segmentation, Optical Neural Networks, Texture Discrimination, Image Processing, FLIR Images, Optical Pattern Recognition

NUMBER OF PAGES: 27

Unclassified	Unclassified	Unclassified	UL

GENERAL INSTRUCTIONS FOR COMPLETING SF 298

The Report Documentation Page (RDP) is used in announcing and cataloging reports. It is important that this information be consistent with the rest of the report, particularly the cover and title page. Instructions for filling in each block of the form follow. It is important to ***stay within the lines*** to meet ***optical scanning requirements***.

Block 1. Agency Use Only *(Leave blank)*.

Block 2. Report Date. Full publication date including day, month, and year, if available (e.g. 1 Jan 88). Must cite at least the year.

Block 3. Type of Report and Dates Covered. State whether report is interim, final, etc. If applicable, enter inclusive report dates (e.g. 10 Jun 87 - 30 Jun 88).

Block 4. Title and Subtitle. A title is taken from the part of the report that provides the most meaningful and complete information. When a report is prepared in more than one volume, repeat the primary title, add volume number, and include subtitle for the specific volume. On classified documents enter the title classification in parentheses.

Block 5. Funding Numbers. To include contract and grant numbers; may include program element number(s), project number(s), task number(s), and work unit number(s). Use the following labels:

C	- Contract	PR	- Project
G	- Grant	TA	- Task
PE	- Program Element	WU	- Work Unit Accession No.

Block 6. Author(s). Name(s) of person(s) responsible for writing the report, performing the research, or credited with the content of the report. If editor or compiler, this should follow the name(s).

Block 7. Performing Organization Name(s) and Address(es). Self-explanatory.

Block 8. Performing Organization Report Number. Enter the unique alphanumeric report number(s) assigned by the organization performing the report.

Block 9. Sponsoring/Monitoring Agency Name(s) and Address(es). Self-explanatory.

Block 10. Sponsoring/Monitoring Agency Report Number. *(If known)*

Block 11. Supplementary Notes. Enter information not included elsewhere such as: Prepared in cooperation with...; Trans. of ...; To be published in.... When a report is revised, include a statement whether the new report supersedes or supplements the older report.

Block 12a. Distribution/Availability Statement. Denotes public availability or limitations. Cite any availability to the public. Enter additional limitations or special markings in all capitals (e.g. NOFORN, REL, ITAR).

- **DOD** - See DoDD 5230.24, "Distribution Statements on Technical Documents."
- **DOE** - See authorities.
- **NASA** - See Handbook NHB 2200.2.
- **NTIS** - Leave blank.

Block 12b. Distribution Code.

- **DOD** - Leave blank.
- **DOE** - Enter DOE distribution categories from the Standard Distribution for Unclassified Scientific and Technical Reports.
- **NASA** - Leave blank.
- **NTIS** - Leave blank.

Block 13. Abstract. Include a brief *(Maximum 200 words)* factual summary of the most significant information contained in the report.

Block 14. Subject Terms. Keywords or phrases identifying major subjects in the report.

Block 15. Number of Pages. Enter the total number of pages.

Block 16. Price Code. Enter appropriate price code *(NTIS only)*.

Blocks 17. - 19. Security Classifications. Self-explanatory. Enter U.S. Security Classification in accordance with U.S. Security Regulations (i.e., UNCLASSIFIED). If form contains classified information, stamp classification on the top and bottom of the page.

Block 20. Limitation of Abstract. This block must be completed to assign a limitation to the abstract. Enter either UL (unlimited) or SAR (same as report). An entry in this block is necessary if the abstract is to be limited. If blank, the abstract is assumed to be unlimited.

* U.S. GPO 1990-0-273-271

NOTICE

When Government drawings, specifications, or other data are used for any purpose other than in connection with a definitely Government-related procurement, the United States Government incurs no responsibility or any obligation whatsoever. The fact that the Government may have formulated or in any way supplied the said drawings, specifications, or other data, is not to be regarded by implication, or otherwise in any manner construed, as licensing the holder, or any other person or corporation; or as conveying any rights or permission to manufacture, use, or sell any patented invention that may in any way be related thereto.

This technical report has been reviewed and is approved for publication.

KEVIN W. AYER, CAPT, USAF
E-O techniques Group
Electro-Optics Branch

DONALD L. TOMLINSON, Chief
E-O Techniques Group
Electro-Optics Branch

FOR THE COMMANDER

GALE D. URBAN, Chief
Electro-Optics Branch
Mission Avionics Division
Avionics Directorate

If youi address has changed, if you wish to be removed from our mailing list, or if the addressee is no longer employed by your organization, please notify WL/AARI-2, Wright-Patterson AFB OH 45433-6543, to help maintain a current mailing list.

Copies of this report should not be returned unless return is required by security considerations, contractual obligations, or notice on a specific document.

TABLE OF CONTENTS

SECTION		PAGE
Abstract		1
1.	Introduction	2
2.	Texture Segmentation Filters	3
3.	Set-Up for Optical Segmentation	9
4.	Segmentation Results	11
5.	Conclusion	17
6.	Acknowledgements	19
7.	References	20

TABLE OF FIGURES

FIGURE		PAGE
1.	Neural Network Based Automatic Target Recognizer	5
2a.	Example of 2-D Cosine Gabor Function	5
2b.	2-D Fourier Transform of (2a)	5
3a.	Cosine CGH Gabor Filter Image	6
3b.	3-D Intensity profile of (3a)	6
4.	Digital Representation of Transmission Function of Symmetric Circular Apertures	6
5a.	Sideview: Digital Representation of Intensity Function of an Airy Disc Wavelet	10
5b.	Topview: Digital Representation of Intensity Function of an Airy Disc Wavelet	10
6.	Wavelet Spectral Images of Pinhole Filters	10
7.	Experimental Set-Up for Optical Segmentation	13
8.	Example of a Template Slide Correlated with a Poorly Chosen Wavelet Using a Pinhole Filter with Apertures Chosen Too Small	13
9.	Wavelet Correlation of a Truck template Slide Using Five Different Pinhole Filters	15
10.	Wavelet Correlation of a Multiple Object template Slide Using a Multiple Orientation Pinhole Filter	15
11.	Segmentation of Static FLIR Image REFJ16 Using a Pinhole Filter	16
12.	Optical Set-Up Used for Observing Segmented and Unsegmented Real-Time FLIR Images Synchronously	16
13.	Segmentation of Two Frames of Real-Time FLIR Imagery Using a Circular Aperture Pair Filter with Two Orientations, 0° and 90°	18

FOREWORD

This Technical Report was prepared by the Air Force Institute of Technology, School of Engineering, Department of Electrical and Computer Engineering, Signal Processing and Pattern Recognition Function, Air University, Wright-Patterson AFB, OH, in conjunction with the Electro-Optics Techniques Group, Electro-Optics Branch, Mission Avionics Division, Avionics Directorate, Wright-Laboratory, Wright-Patterson AFB, OH.

This Technical Report was submitted by the authors in Oct 1991.

An optical image segmentor using neural based wavelet filtering techniques

Christopher P. Veronin Steven K. Rogers Matthew Kabrisky

Kevin L. Priddy Kevin W. Ayer Byron Welsh

Department of Electrical and Computer Engineering

Air Force Institute of Technology

AFIT/ENG, Wright-Patterson AFB, OH 45433-6583

ABSTRACT

This paper presents a neural based optical image segmentation scheme for locating potential targets in cluttered FLIR images. The advantage of such a scheme is speed, i. e., the speed of light. Such a design is critical to achieve real-time segmentation and classification for machine vision applications. The segmentation scheme used was based on texture discrimination and employed biologically based orientation specific filters (wavelet filters) as its main component. These filters are the well understood impulse response functions of mammalian vision systems from input to striate cortex. By using the proper choice of aperture pair separation, dilation, and orientation, targets in FLIR imagery were optically segmented. Wavelet filtering is illustrated for glass template slides, as well as segmentation for static and real-time FLIR imagery displayed on a liquid crystal television.

Subject Terms: Gabor Transforms, Segmentation, Optical Neural Networks, Texture Discrimination, Image Processing, FLIR Images, Optical Pattern Recognition.

1. INTRODUCTION

Segmentation of potential targets from cluttered images is a critical step before classification of the target can begin. Over the past 25 years, several segmentation algorithms have been developed at the Air Force Institute of Technology (AFIT) [1, 2, 3, 4, 5, 6, 7], however, they are heuristic in nature and use non-linear mathematical manipulation of data—algorithms not readily implemented optically and computationally intense for real-time use. In a recent research effort at AFIT, Gabor filtering techniques were applied in a digital algorithm that successfully segmented Forwarded-Looking Infra Red (FLIR) imagery and provided a linear algorithm that could be applied optically [8]. Gabor functions have been shown to be a good model for the impulse response function of mammalian visual systems [9, 10]. The optical image segmentor presented in this paper adopted a similar linear algorithm as in the digital approach, but also tested a different type of wavelet filter other than the Gabor. The optical implementation allows for instantaneous and automatic segmentation of real-time FLIR imagery for machine vision processing.

Neural network classification schemes at AFIT have incorporated the optical segmentor as a front end processor [11]. Such a scheme is shown in Figure 1. Essentially, the optical segmentor limits the field-of-view of the classification neural network to potential targets in the scene and feeds the classification neural network the wavelet correlation values as discriminant features to process. The neural network shown is a collection of specific neural networks each trained to recognize only one class of objects based on an optimized set of wavelet correlation values. The output of the neural network is then used as feedback to the optical segmentor to generate a customized wavelet filter based on the network's determination of the most probable class of the segmented object. The loop is iteratively processed until a desired threshold is reached or the classification network is no longer able to improve classification capability. Once the classification has been made, the process can be repeated for other items of interest in the correlation plane.

The optical architecture presented uses a liquid crystal television (LCTV) spatial light modulator (SLM) as a grey-scale amplitude modulator for displaying static and real-time FLIR imagery as inputs into the optical setup. Over the past five years, LCTVs have been demonstrated as capable amplitude and phase SLMs in optical image processing setups in various research projects [12, 13, 14, 15, 16, 17, 18, 19, 20, 21]. The main advantage of LCTVs is low cost (approximately $100 to $1200), and their main disadvantage is low resolution (pixel sizes on the order of 370 μm). The low resolution of the LCTV posed some optimization problems in this research effort, but the requirement for grey-scale capability made the LCTV the most suitable choice over other SLMs. The limitations of using an LCTV for this application are discussed. Also note that many of the digitized camera images presented were reversed imaged, i.e., light areas are presented dark and dark areas are presented light. This was done to highlight the areas of interest better.

2. TEXTURE SEGMENTATION FILTERS

The design of the segmentation filters used is based on 2-dimensional Gabor wavelet filtering techniques employed as a digital image processing tool for texture segmentation [22, 23, 9, 24]. The 2-D Gabor wavelet can be described as a modulated Gaussian "window" which possesses the distinct property of maintaining the theoretical lower bound of joint uncertainty in the space/frequency domain [9]. Joint uncertainty refers to the space and frequency resolution of the function. An example of a 2-D cosine Gabor function (space domain) and its 2-D

Fourier transform (frequency domain) is given in Figure 2. In addition, Gabor wavelets have been proposed as good models for the 2-D receptive fields of mammalian visual cortex simple cells (neurons) [9]. In this sense, the optical segmentor presented in this article can truly be called an optical neurocomputer.

One way to understand the segmentation process employed is to think of the filters as "orientation specific, bandpass spatial filters". Orientation specific, bandpass spatial filtering implies frequency discrimination or "textural" discrimination at a specific orientation of the texture. Similar biological processing has been known to exist since 1962 [25]. Optically segmenting distinct textures requires passing their dominant spatial frequencies through symmetric apertures at appropriate separations and orientations and blocking out the rest of the spectrum.

Thus, orientation specific, bandpass spatial filters are nothing more than symmetrically located apertures. The apertures of choice would be symmetrical gaussians, as shown in Figure 2b, in order to take advantage of the lower bound of the joint uncertainty relationship. To this end, gaussian apertures were fabricated during the course of this research using detour-phase computer generated holography (CGH), an example of which is shown in Figure 3 along with its 3-D transmission profile. However, these filters were not easy to fabricate and transmitted too much undesired image spectrum.

A much simpler solution to employing wavelet filtering was to use circular apertures instead of gaussian apertures. In the space domain, one could think of them as Airy disc wavelets. In other words, if we model the circular apertures as having constant intensity across them, then the transmittance function of a symmetric aperture pair can be expressed mathematically in the frequency domain as:

$$\mathrm{T}(\xi,\eta) = \mathrm{circ}\left(\frac{\rho}{(l/2)}\right) * \left[\delta(\xi-\xi_0,\eta-\eta_0) + \delta(\xi+\xi_0,\eta+\eta_0)\right] \tag{1}$$

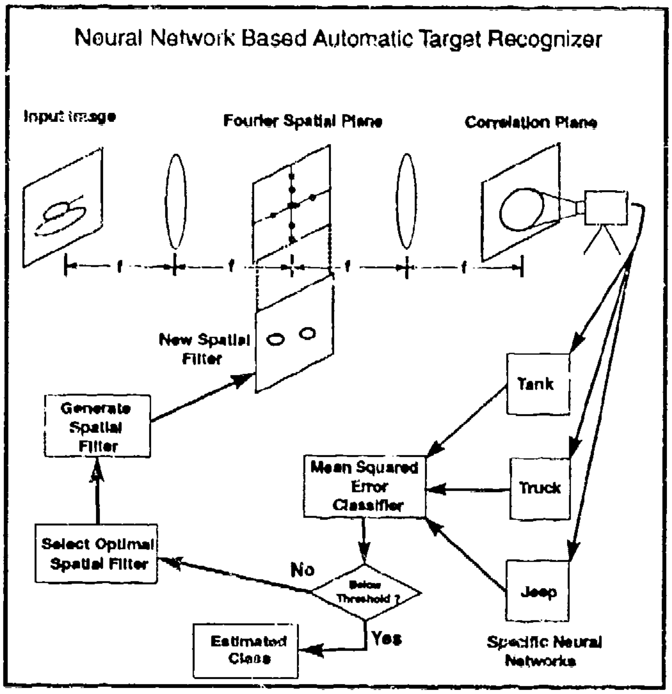

Figure 1: Neural Network Based Automatic Target Recognizer

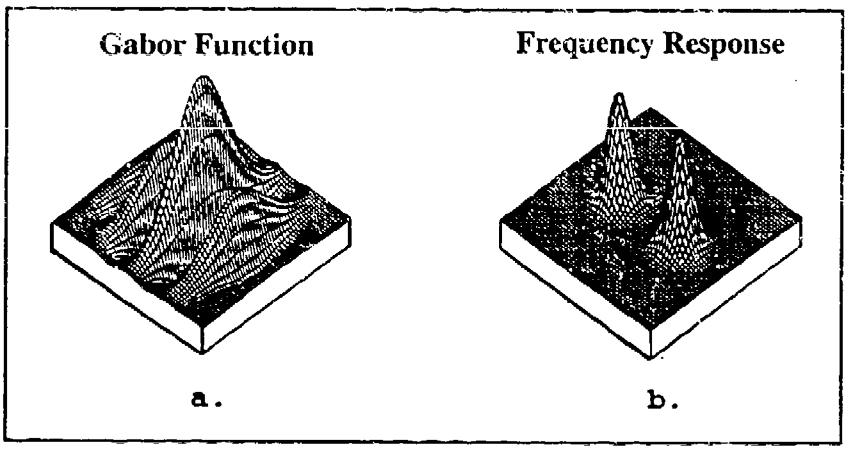

Figure 2: (a) Example of a 2-D cosine Gabor function (b) 2-D Fourier transform of (a)

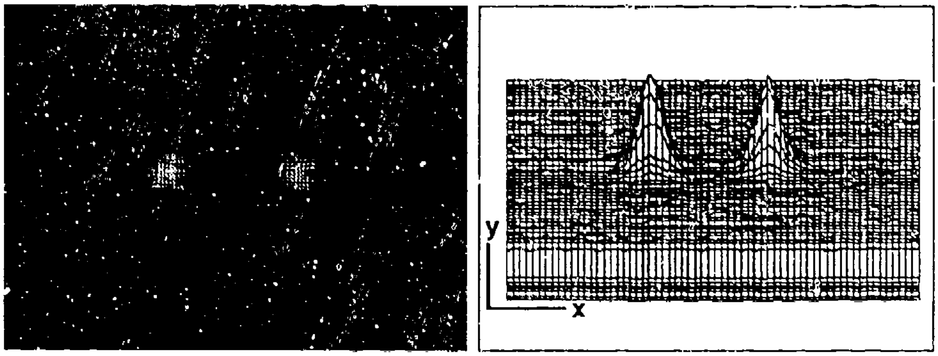

a. **b.**

Figure 3: (a) Cosine CGH Gabor filter image; (b) Its 3-D intensity profile

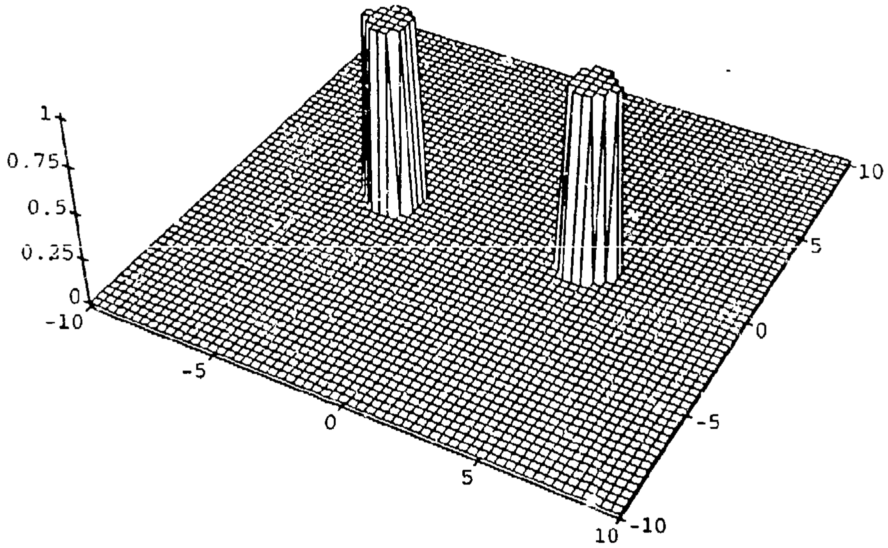

Figure 4: Digital representation of the transmission function of symmetric circular apertures

where:

$$\mathrm{circ}\left(\frac{\rho}{(l/2)}\right) = \begin{cases} 1 & \rho \le l/2 \\ 0 & \text{otherwise} \end{cases} \tag{2}$$

"*" represents a convolution, δ represents a delta function, $\rho = \sqrt{\xi^2 + \eta^2}$, ξ_0 represents a distance along the ξ direction, η_0 represents a distance along the η direction, and l represents the circular dilation (diameter). A 2-D digital representation of the transmission function of symmetric circular apertures is shown in Figure 4.

The "inverse" Fourier transform of the symmetric circular aperture pair can be expressed mathematically in the space domain as an Airy disc wavelet:

$$\mathrm{t}(x, y) = \left(\frac{l}{2}\right)^2 \frac{\mathbf{J_1}(\pi l r)}{(l r/2)} \cos\left(2\pi(\xi_0 x + \eta_0 y)\right) \tag{3}$$

where, $r = \sqrt{x^2 + y^2}$ and $\mathbf{J_1}$ represents a first-order Bessel function.

Furthermore, Goodman [26] derived the intensity of an Airy disc which, combined with the square of the sinusoid, gives the intensity function of the Airy disc wavelet:

$$\mathrm{I}(x, y) = |\mathrm{t}(x, y)|^2 = \left[2\frac{\mathbf{J_1}(\pi l r/\lambda f)}{(\pi l r/\lambda f)}\right]^2 \left[\cos\left(2\pi(\xi_0 x + \eta_0 y)\right)\right]^2 \tag{4}$$

A 2-D digital representation of the intensity function of an Airy disc wavelet is shown in Figure 5. The figure shows both a side view and a view looking straight down. The middle lobe was clipped at the top in order to emphasize the side lobe oscillations more, however, at full scale the first side lobe of an Airy disc function is less than 2% of the amplitude of the middle lobe.

Using Equation 4, the number of cycles in the middle lobe of the Airy disc can be predicted. If r_0 is the distance from the origin to the first zero crossing of the Airy disc, then

$$r_0 = \frac{1.22\lambda f}{l} \tag{5}$$

Additionally, the spatial frequency of the wavelet can be given in terms of

$$2\xi_0 = \frac{2\rho}{\lambda f} \tag{6}$$

Thus, the number of cycles over the total lobe can be calculated from Equations 5 and 6 as:

$$\frac{\#\text{cycles}}{\text{centerlobe}} = 2r_0 2\xi_0 = \frac{4.88\rho}{l} \tag{7}$$

For example, if the aperture separation is 2 mm ($\rho = 1$ mm) and the aperture dilation, l, is 1 mm, then the number of cycles per middle Airy disc lobe should be 4.88 cycles/lobe. Note that this result is independent of the wavelength of the laser or the focal length of the lens.

Recall that the Gabor wavelet (modulated gaussian) was the best choice of filter for mathematical reasons; however, the Airy disc wavelet was chosen as a filter because it was easy to implement optically, and its central lobe approximated a Gabor wavelet well. The central lobe of a gaussian function and an Airy pattern (the envelopes of the wavelets in the space domain) have similar shapes, and although the Airy pattern possesses sidelobes which comprise about 16% of its intensity [27], the intensity is well distributed between them resulting in their having little or no effect in the correlation output.

The implementation of the symmetric circular aperture filters was trivial and only required that some medium be placed in the filter plane that could be impressed with small circular apertures (pinholes) to pass the desired spectral coefficients and block the rest of the image spectrum. The medium of choice was heavy, black aluminum foil, since it was readily available, required no special tools or software to manipulate (i.e., drill press or computer), and retained its shape fairly well (some slight microscopic tearing was unavoidable). The filters were made by cutting and smoothing 5 cm x 5 cm pieces of foil, then impressing circular aperture pairs into them using a pin. The apertures were placed along a common axis symmetrical to an origin (middle of the foil). Separations of apertures varied from 2 mm to 12 mm. Diameters of apertures varied from about 0.5 mm to 3 mm. Orientations were not limited since the filters were placed in a rotating mount with a 360° range. Figure 6 shows four different wavelet spectral images recorded from an optical bench from four different pinhole pair filters and demonstrates the effect of changing aperture separation, dilation, and orientation. An alternative to a fixed filter approach is to use an electronically addressed binary magneto-optic SLM which would allow for real-time filter selection, as implied by Figure 1.

3. SETUP FOR OPTICAL SEGMENTATION

The basic setup used to perform optical segmentation is given in Figure 7. Input images were placed at P_o, and spatial filters were placed at P_t. The only difference between this setup and a general spatial filtering 4-f setup is two extra lenses which increase the size of the input image spectrum incident on the spatial filter at P_t. Hence, this setup could be called an 8-f setup. An increase in the spectrum size allows the individual spatial frequencies (diffraction orders) to be identified and segmented more easily. For example, the relationship between input image spatial frequency and spectrum location is

$$f_x = x_f/\lambda f \tag{8}$$

where f_x is the x-component of the spatial frequency, x_f is the x-component of the spectrum location, λ is the

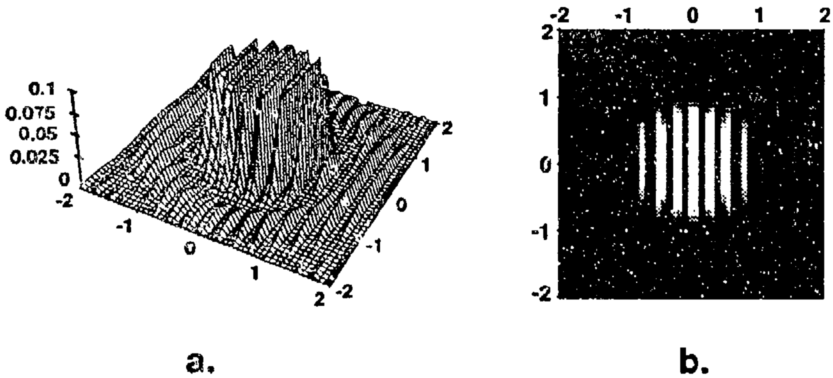

Figure 5: Digital representation the intensity function cf an Airy disc wavelet at given at two viewpoints: (a) sideview; (b) topview

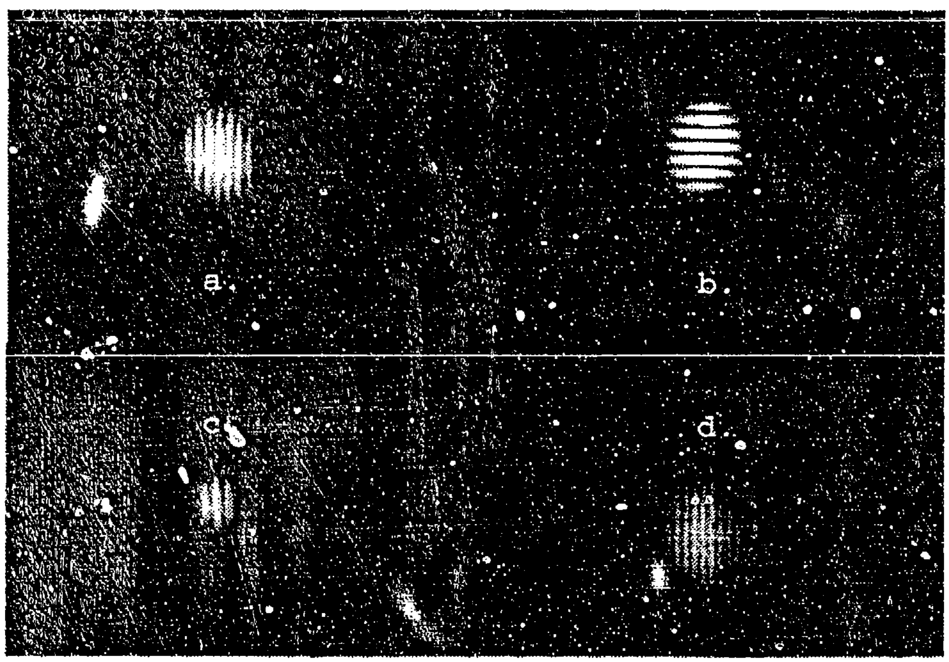

Figure 6: Wavelet spectral images of pinhole filters: (a) separation=2 mm dilation=.5 mm, orientation=0°; (b) 2,.5,90°; (c) 2,1,0°; (d) 4,.5,0°

wavelength of the source, and f is the focal length of the lens. Thus, if $f_x = 10$ cycles/cm, $\lambda = 488.0$ nm, and $f = 300$ mm, then $x_f = 0.146$ mm, which is physically too small to segment easily. However, if we magnify x_f, say $7.5x$, it has a dimension of 1.01 mm, which is more easily segmented.

An argon-ion laser ($\lambda = 488.0$ nm) was used for the coherent light source. The beam was collimated to a 3 1/2 inch diameter with a $10x$ microscope objective, a 15 μm pinhole, and a 150 mm focal length, 5 1/2 inch diameter lens in order to use as much of the LCTV screen as possible (the LCTV was a modified Sony Video Walkman and had a 4 inch diagonal screen). The final setup configuration had 300 mm compound lenses for L_1, L_3, and L_4, and a simple 40 mm convex lens for L_2. Thus, the magnification of the spectrum was $7.5x$. An iris placed in front of L_1 served as an aperture stop and cut down on the high frequency interference between pixels when the LCTV was used as an input device. A Sony CCD camera was placed at P_i to record the output images. The camera was connected to an AT&T TARGA framegrabber in a Zenith 286 computer.

4. SEGMENTATION RESULTS

Wavelet correlation results for template slides and segmentation results for static and real-time FLIR imagery displayed on the LCTV are presented. The template slides of trucks, tanks, and jeeps are essentially "pre-segmented", since they consist of constant intensity silhouettes with no background clutter. However, they provide a good transition to understanding the segmentation of the FLIR images by observing how aperture separations and dilations control the resulting wavelet correlation. Template slide correlation was accomplished with pinhole pair filters implemented on heavy, black aluminum foil and detour-phase computer generated holograms.

Proper aperture dilation which corresponds to wavelet localization was found to be of utmost importance to obtain highly detailed edge enhanced images. If the aperture dilation was chosen too small, its corresponding wavelet overshadowed any detail in the input image. For example, a first try at correlating a "small" truck shown in Figure 8a was to use a pinhole pair filter with 2 mm separations, 0.5 mm dilations, and different orientations of 0°, 90°, and a combination of both resulting in the wavelet projection shown in Figures 8b–d, respectively. Figures 8b and c show wavelets correlating on edges in the truck image; however, the wavelets are so large that they overshadow any detail within the correlated image and interfere with one another. Hence, the correlation that resulted from the combined filter shown in Figure 8d had hardly any resemblance to the input image.

The best combination filter for wavelet decomposition of the small truck template was found to be a pinhole pair filter with 6 mm separations, 3 mm dilations, and orientations of 30, 90, and 150°. The orientations were chosen in order to optimize the space available on the filter. Once the optimal filter was determined, a permanent filter was fabricated by drilling the circular apertures into 1/16 inch aluminum squares. A highly detailed edge enhancement of the small truck template slide was achieved using this filter. This result is shown in Figure 9f. Note the fine detail along the edges due to the more localized wavelet produced by the filter. Also note that the back edge of the truck was not enhanced. This was due to the filter not having a 0° orientation and illustrates the high degree of sensitivity the filter has to orientation.

The other pictures in Figure 9 are for comparison purposes and show less than optimal wavelet selections for the small truck (Figure 9a) using different filter configurations of aperture separation and dilation. Figure 9b is the same image as Figure 8b. It came from correlating the image with a pinhole pair having 2 mm separations, 0.5 mm dilations, and orientations of 0 and 90°. Figure 9c came from correlating the image with a pinhole pair having 2 mm separations, 1 mm dilations, and orientations of 0 and 90°. Figure 9d came from correlating the image with a pinhole pair having 4 mm separations, 2 mm dilations, and orientations of 0 and 90°. Figure 9e came from correlating the image with a pinhole pair having 6 mm separations, 1 mm dilations, and orientations of 0, 45, 135, and 90°. Note that the detail in Figure 9d is better than that in Figure 9e. Hence, it appears that

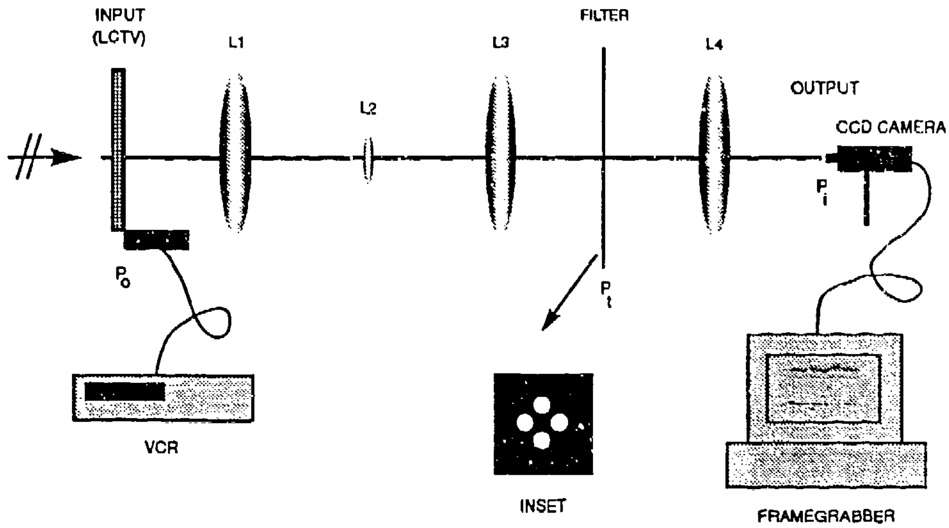

Figure 7: Experimental setup for optical segmentation. The inset is an orientation specific, bandpass spatial filter with circular apertures.

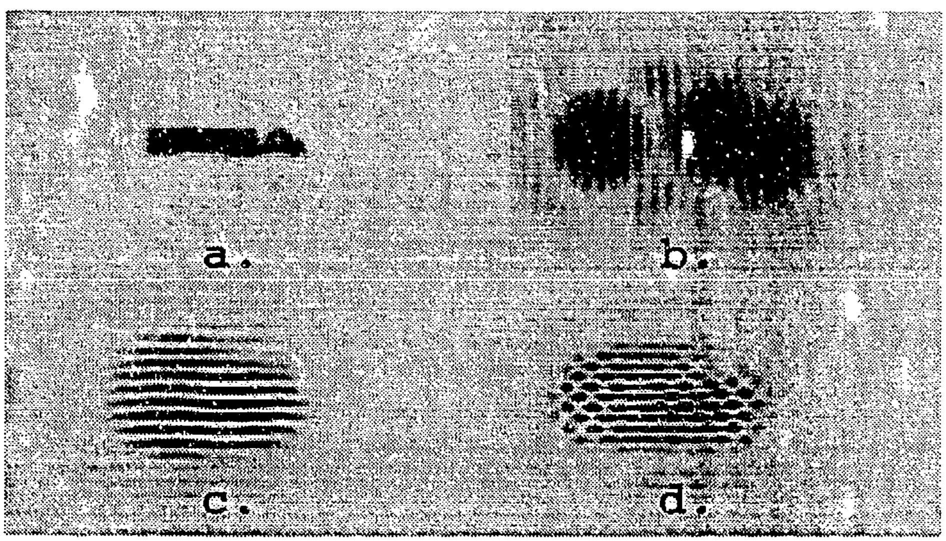

Figure 8: Example of a template slide correlated with a poorly chosen wavelet using a pinhole filter with apertures chosen too small. (a) image of template slide; (b) Correlation result using pinhole filter at 0° orientation; (c) Correlation result using pinhole filter at 90° orientation; (d) Correlation result using pinhole filter at both 0 and 90° orientations

dilation is more important than frequency for achieving highly detailed correlations.

As a final example of wavelet correlation with template slides using circular apertures, Figure 10 shows a finely detailed projection of a multiple object template slide consisting of a truck, a jeep, and two tanks using the 6 mm separation, 3 mm dilation, multiple orientation pinhole pair filter described for the correlation in Figure 9f above.

An example of static FLIR segmentation using a FLIR image displayed onto the LCTV and a permanent pinhole filter on an aluminum square with 4 mm aperture separations, 2 mm aperture dilations, and two orientations of 0 and 90° is shown in Figure 11.

The segmented images are not as detailed as the ones obtained in the template testing because pinhole separations were limited to 4 mm and pinhole dilations were limited to 2 mm due to the low resolution of the LCTV. This is the same filter that was used for segmentation in Figure 9d. In other words, the pinhole dilations could not have been made any wider without passing the higher order periodic spectrums of the LCTV and prevent the segmentation [28].

The real-time FLIR imagery was segmented using the same permanent circular aperture filter as was used for static FLIR segmentation. A split-screen video tape was made showing the unsegmented FLIR tape on the upper left-hand corner of the screen and the segmented image on the upper right-hand corner of the screen. Figure 12 shows the optical configuration used to observe both the segmented and unsegmented real time FLIR images synchronously, using a beamsplitter placed just before the filter, a second lens, a second CCD camera, and a quad input video processor. The second lens, L_5, had a focal length of 250 mm, which was smaller than the 300 mm focal length of L_4. Hence, the unsegmented FLIR image scene is shown slightly smaller than the segmented FLIR

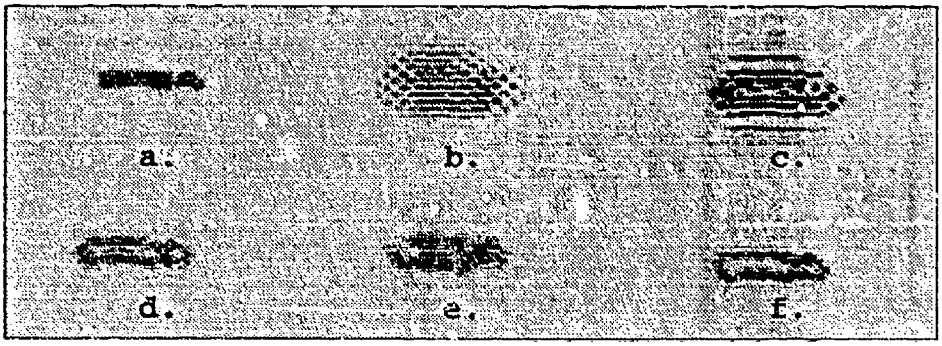

Figure 9: Wavelet correlation of a truck template slide using five different pinhole filters. (a) image of template slide; (b) separations = 2 mm, dilations = .5 mm, orientations = 0 and 90°; (c) s = 2 mm, d = 1 mm, o = 0 and 90°; (d) s = 4 mm, d = 2 mm, o = 0 and 90°; (e) s = 6 mm, d = 1 mm, o = 0, 45, 90, and 135°; (f) s = 6 mm, d = 3 mm, o = 30, 90, and 150°

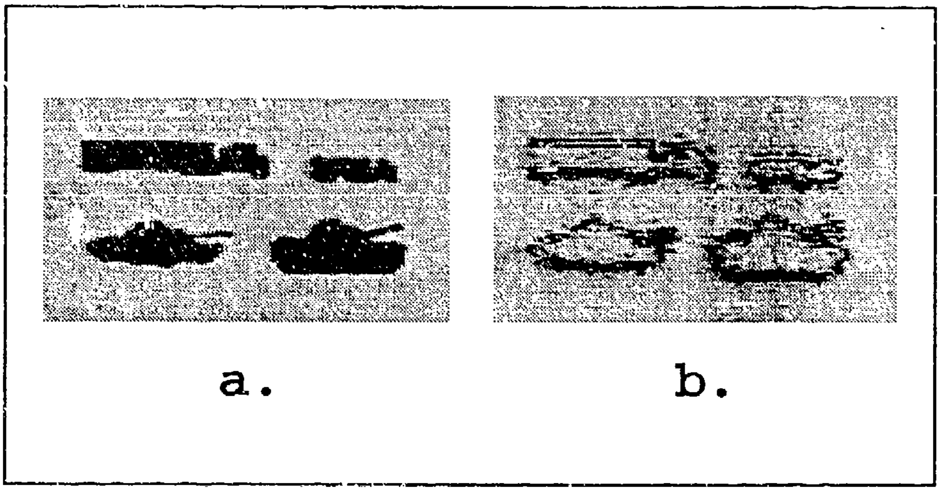

Figure 10: Wavelet correlation of a multiple object template slide using a multiple orientation pinhole filter. (a) image of template slide; (b) correlation result

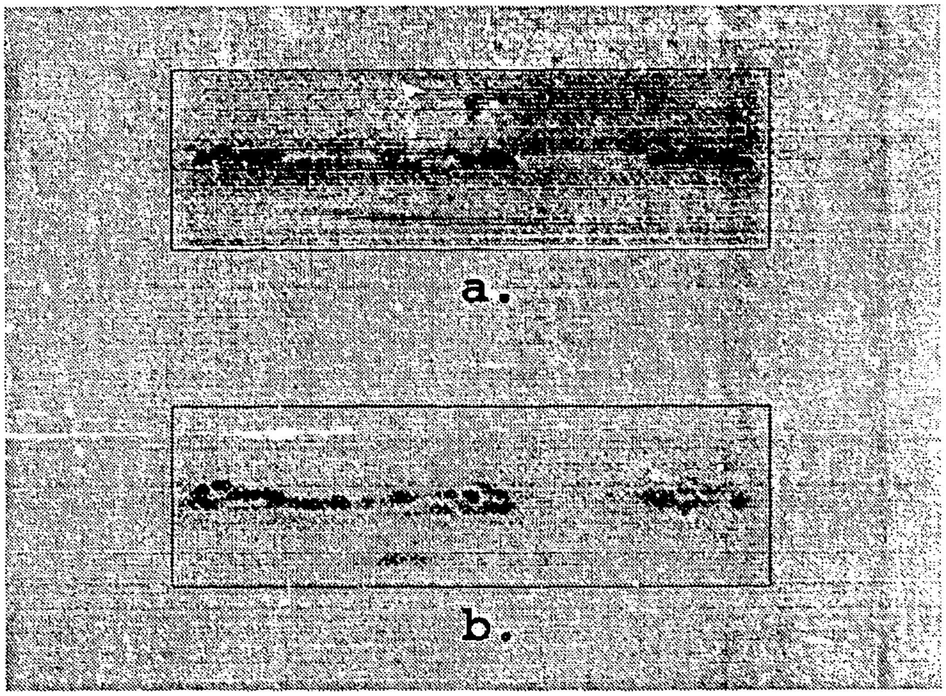

Figure 11: Segmentation of static FLIR image REFJ16 using a pinhole filter. (a) original FLIR image; (b) segmented image

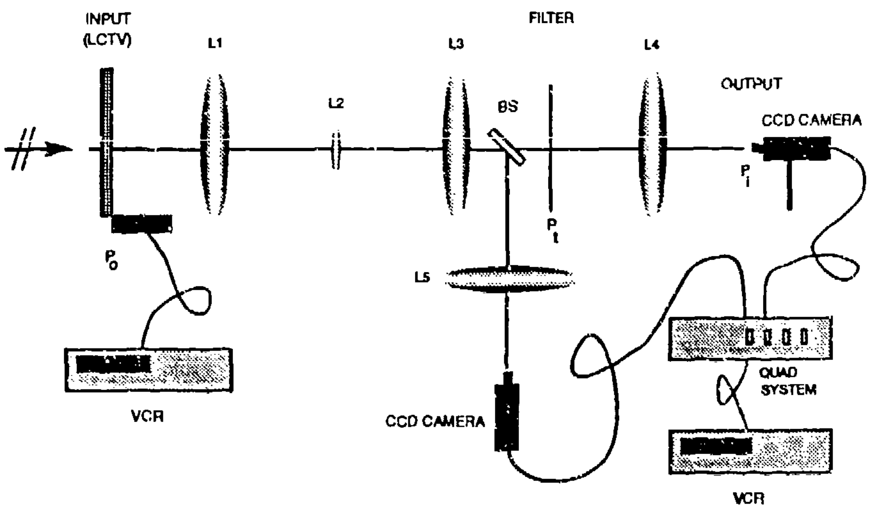

Figure 12: Optical setup used for observing segmented and unsegmented real time FLIR images synchronously

image.

In this forum, the real power of optical segmentation can be observed and appreciated, because of its ability to perform instantaneous two-dimensional Fourier transforms. A similar digital segmentation algorithm would be bogged down very quickly trying to calculate Fast Fourier transforms (FFT's) and inverse FFT's at 30 frames/sec. Two digitized frames of the video (not consecutive) are shown in Figure 13. Noise around the edges of the circular window was inherent noise from the lenses and the LCTV screen. When seen in real time, these noisy bright spots are constant and don't change (compare noise around edge in segmented FLIR image, frame 1 to noise around edge in segmented FLIR image, frame 2). Further post-processing of the segmented FLIR imagery could be accomplished to remove this constant noise factor.

5. CONCLUSION

In this paper we have presented an automatic, optically based image segmentation scheme for static and real-time FLIR imagery displayed on an LCTV. The segmentation scheme used was based on texture discrimination and employed neural based orientation specific, bandpass spatial filters (wavelet filters) as its main component. By using the proper choice of aperture pair separation, dilation, and orientation, potential targets in FLIR imagery were optically segmented using spatial filtering techniques. The output of the system is a correlation of the input image with the wavelet filter. Neural network classifiers at AFIT are incorporating the optical neural based segmentor as a front end processor which can determine the locations of potential targets and feed the classification neural network with the correlation peaks for their input data.

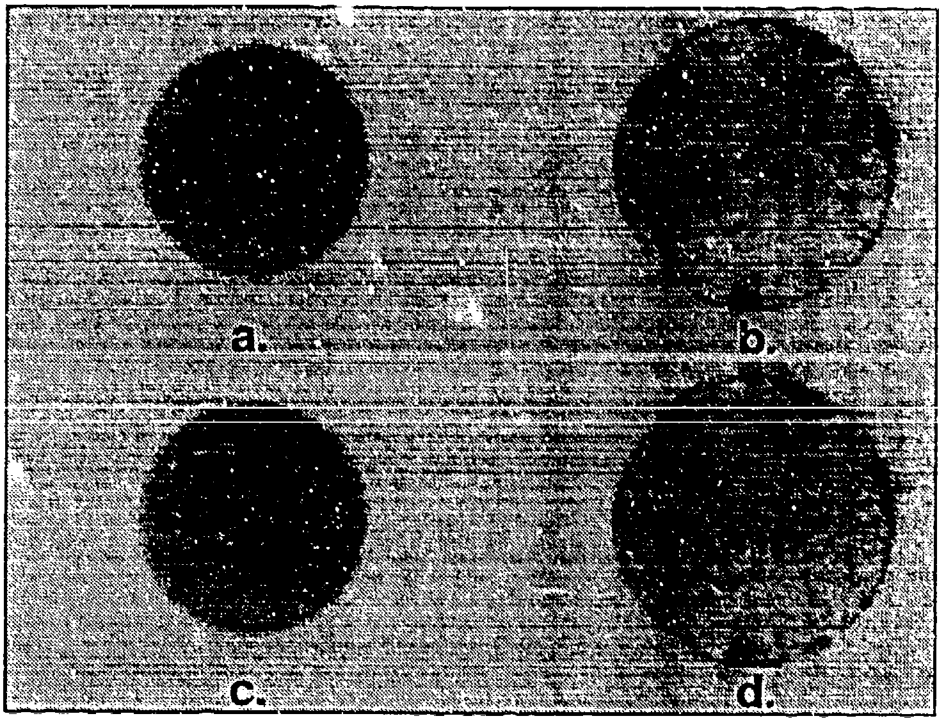

Figure 13: Segmentation of two frames of real-time FLIR imagery using a circular aperture pair filter with two orientations, 0 and 90°. (a) original FLIR image, frame 1; (b) segmented FLIR image, frame 1; (c) original FLIR image, (d) bottom right: segmented FLIR image, frame 2

6. ACKNOWLEDGEMENTS

This work was supported by funding through Capt Kevin Ayer from the Electro-Optic Lab at Wright Labs/AARI-2 and the Rome Air Development Center RL/IRRA.

7. References

[1] L. F. Bush, "The design of an optimum alphanumeric symbol set for cockpit displays," Master's thesis, School of Engineering, Air Force Institute of Technology (AU), Wright-Patterson AFB OH, Dec. 1977.

[2] N. A. Hamadani, "Automatic target cueing in ir imagery," Master's thesis, School of Engineering, Air Force Institute of Technology (AU), Wright-Patterson AFB OH, Dec. 1981.

[3] M. Horev, "Picture correlation model for automatic machine recognition," Master's thesis, School of Engineering, Air Force Institute of Technology (AU), Wright-Patterson AFB OH, Dec. 1980.

[4] R. E. Roberts, M. Kabrisky, S. K. Rogers, and E. Amburn, "Three dimensional scene analysis using stereo based imaging," in *Proceedings of the SPIE Sixth Annual Conference on Applications of Artificial Intelligence, Volume 937*, (Bellingham, WA), pp. 280–286, SPIE Press, 1988.

[5] M. C. Roggemann, *Multiple Sensor Fusion for Detecting Targets in FLIR and Range Images*. PhD thesis, School of Engineering, Air Force Institute of Technology (AU), Wright-Patterson AFB OH, June 1989.

[6] D. W. Ruck, S. K. Rogers, and M. Kabrisky, "Multisensor target detection and classification," in *Proceedings of the SPIE Conference on Infrared Sensors and Sensor Fusion, Volume 931*, (Bellingham, WA), pp. 14–21, SPIE Press, 1988.

[7] C. Tong, S. K. Rogers, J. P. Mills, and M. Kabrisky, "Multisensor data fusion of laser and forward looking infrared (flir) for target segmentation and enhancement," in *Proceedings of the SPIE Conference on Infrared Sensors and Sensor Fusion, Volume 782*, (Bellingham, WA), pp. 10–19, SPIE Press, 1987.

[8] K. Ayer, S. K. Rogers, M. Kabrisky, and M. Oxley, "Forward looking infrared image segmentation and pattern recognition using gabor transforms and joint transform correlation techniques," *Opt Eng*, 1991. submitted for publication.

[9] J. G. Daugman, "Complete discrete 2-d gabor transforms by neural networks for image analysis and compression," *IEEE Transactions on Acoustics, Speech, and Signal Processing*, vol. 36, pp. 1169–1179, July 1988.

[10] J. P. Jones and L. A. Palmer, "An evaluation of the two dimensional gabor filter model of simple receptive fields in cat striate cortex," *Journal of Neurophysiology*, vol. 58, pp. 1233–1258, December 1987.

[11] K. L. Priddy, S. K. Rogers, M. Kabrisky, B. Welsh, and J. Jones Jr., "Image segmentation, feature extraction, and classification using neural networks," in *Proceedings of the Sixth Annual Aerospace Applications of Artificial Intelligence Conference*, ACM Press, 1990.

[12] T. H. Barnes, T. Eiju, K. Matusada, and N. Ooyama, "Phase-only modulation using a twisted nematic liquid crystal television," *Applied Optics*, vol. 28, pp. 4845–4852, November 1989.

[13] D. A. Gregory, "Real-time pattern recognition using a modified liquid crystal television in a coherent optical correlator," *Applied Optics*, vol. 25, pp. 467–469, February 1986.

[14] K. D. Hughes, S. K. Rogers, J. P. Mills, and M. Kabrisky, "Optical preprocessing using liquid crystal televisions," *Applied Optics*, vol. 26, pp. 1042–1044, March 1987.

[15] Y. Li, A. Kostrzewski, D. H. Kim, and G. Eichmann, "Liquid crystal tv-based white light optical tracking novelty filter," *Applied Optics*, vol. 28, pp. 4861–4864, November 1989.

[16] H.-K. Liu, J. A. Davis, and R. A. Lilly, "Optical-data-processing properties of a liquid-crystal television spatial light modulator," *Optics Letters*, vol. 10, pp. 635–637, December 1985.

[17] H.-K. Liu and T.-H. Chao, "Liquid crystal television spatial light modulators," *Applied Optics*, vol. 28, pp. 4772–4780, November 1989.

[18] K. Lu and B. E. A. Saleh, "Theory and design of the liquid crystal tv as an optical spatial light modulator," *Optical Engineering*, vol. 29, pp. 240–246, March 1990.

[19] O. Perez and M. A. Karim, "An efficient implementation of joint fourier transform correlation using a modified lctv," *Microwave and Optical Technology Letters*, vol. 2, pp. 193–196, June 1989.

[20] E. C. Tam, F. T. S. Yu, D. A. Gregory, and R. D. Juday, "Autonomous real-time object tracking with an adaptive joint transform correlator," *Optical Engineering*, vol. 29, pp. 314–320, April 1990.

[21] F. T. S. Yu, S. Jutamulia, T. W. Lin, and D. A. Gregory, "Adaptive real-time pattern recognition using a liquid crystal tv based joint transform correlator," *Applied Optics*, vol. 26, pp. 1370–1372, April 1987.

[22] K. W. Ayer, "Gabor transforms for forward looking infrared image segmentation," Master's thesis, School of Engineering, Air Force Institute of Technology (AU), Wright-Patterson AFB OH, Dec. 1989.

[23] A. C. Bovik, M. Clark, and W. S. Geisler, "Multichannel texture analysis using localized spatial filters," *IEEE Transactions on Pattern Analysis and Machine Intelligence*, vol. 12, pp. 55–73, January 1990.

[24] M. R. Turner, "Texture discrimination by gabor functions," *Biological Cybernetics*, vol. 55, pp. 71–82, 1986.

[25] D. Hubel and T. Wiesel, "Receptive fields, binocular interaction, and functional architecture in the cat's visual cortex," *Journal of Physiology (London)*, vol. 160, pp. 106–154, 1962.

[26] J. W. Goodman, *Introduction to Fourier Optics*. New York: McGraw-Hill Book Company, 1968.

[27] E. Hecht, *Optics*. Reading, Mass.: Addison-Wesley Publishing Company, Inc., 1988.

[28] C. P. Veronin, S. K. Rogers, M. Kabrisky, B. Welsh, K. L. Priddy, and K. W. Ayer, "An optical image segmentor using wavelet filtering techniques as the front end of a neural network classifier," in *Proceedings of the SPIE 1991 International Symposium and Exhibition on Optical Engineering and Photonics in Aerospace Sensing*, (Bellingham, WA), SPIE Press, 1991.